Oceanic Isopycnal Slope Spectra. Part II: Turbulence

JODY M. KLYMAK

Scripps Institution of Oceanography, University of California, San Diego, La Jolla, California

JAMES N. MOUM

College of Oceanic and Atmospheric Sciences, Oregon State University, Corvallis, Oregon

(Manuscript received 3 November 2005, in final form 26 July 2006)

ABSTRACT

Isopycnal slope spectra were computed from thermistor data obtained using a microstructure platform towed through turbulence generated by internal tidal motions near the Hawaiian Ridge. The spectra were compared with turbulence dissipation rates ε that are estimated using shear probes. The turbulence subrange of isopycnal slope spectra extends to surprisingly large horizontal wavelengths (>100 m). A four-order-of-magnitude range in turbulence dissipation rates at this site reveals that isopycnal slope spectra $\propto \varepsilon^{2/3}k_x^{1/3}$. The turbulence spectral subrange ($k_x > 0.4$ cpm) responds to the dissipation rate as predicted by the Batchelor model spectrum, both in amplitude and towed vertical coherence. Scales between 100 and 1000 m are modeled by a linear combination of internal waves and turbulence while at larger scales internal waves dominate. The broad bandwidth of the turbulence subrange means that a fit of spectral amplitude to the Batchelor model yields reasonable estimates of ε, even when applied at scales of tens of meters that in vertical profiles would be obscured by other fine structure.

1. Introduction

Turbulence in the ocean enhances mixing of tracers and momentum by creating small-scale variance that increases gradients across which molecular diffusion acts. In the ocean's interior, turbulence is usually thought to be the result of breaking small-scale internal waves. Much effort has gone into estimating the rate of turbulence dissipation in the ocean, either by direct measurement (Osborn and Cox 1972), or by characterizing the internal wave field and assuming that the rate of energy lost from it is a predictable function of its strength (Henyey et al. 1986).

In this paper, isopycnal slope spectra[1] collected in the deep ocean near the Hawaiian Ridge are fit to a simple internal wave model and the Batchelor spectrum for turbulence (Batchelor 1959). Slope spectra are thought to be dominated by internal waves at low wavenumbers but, since the vertical-to-horizontal aspect ratio of internal waves is small, their influence on horizontal slope spectra does not extend to as high wavenumbers as in vertical strain spectra (Klymak and Moum 2007, hereinafter Part I). Conversely, the signature of turbulence extends to lower wavenumbers in horizontal than in vertical spectra (Fig. 1).

There is a substantial literature describing horizontal temperature spectra in the ocean, much of it overlapping the scales discussed here (McKean and Ewart 1974; Katz 1975; Katz and Briscoe 1979; Marmorino 1987; Dugan et al. 1986). These spectra share many of the characteristics of the spectra sketched in Fig. 1b, slightly red at low wavenumbers and blue at high wavenumbers. The low wavenumbers in these spectra have usually been interpreted as internal waves, and they inspired early versions of the empirical spectrum of internal waves (hereinafter referred to as GM75; Garrett and Munk 1975). It was also recognized that the shape and amplitude at high wavenumbers were likely set by turbulence. Patches of high temperature variance have

[1] We cast our spectra in terms of gradients, made in the direction of measurement, of vertical isopycnal displacements ζ. The vertical gradient, measurable from a vertical profiler, is the vertical strain ζ_z. The horizontal gradient, measurable from a towed instrument, is the isopycnal slope ζ_x.

Corresponding author address: J. Klymak, School of Earth and Ocean Sciences, University of Victoria, P.O. Box 3055, STN CSC, Victoria, BC V8W 3P6, Canada.
E-mail: jklymak@ uvic.ca

DOI: 10.1175/JPO3074.1

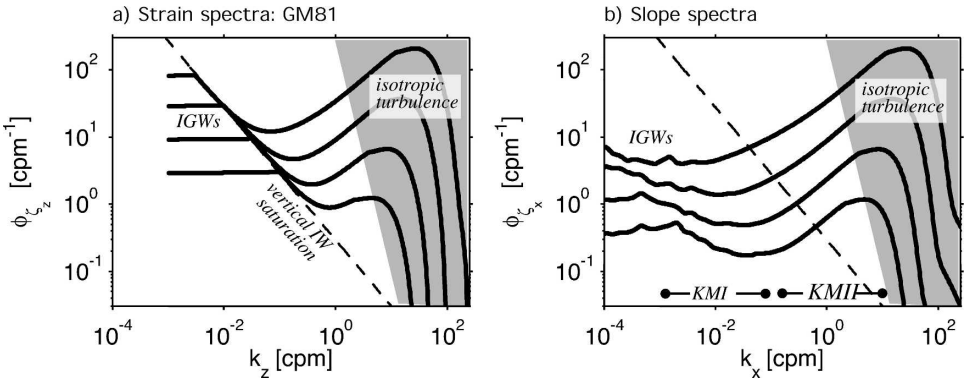

FIG. 1. (a) Strain spectra with saturated internal wave subrange and turbulence for four different energy levels and their corresponding turbulence levels assuming $\varepsilon \sim E^2$, after D'Asaro and Lien (2000) except the turbulence is added to the internal wave spectrum rather than intersecting them with a sharp change of slope. (b) Slope spectra in the same wave and turbulence fields: the slope spectra have been computed from the vertical assuming a frequency spectrum with a large M_2 component as described in Part I (KMI). (The slightly jagged nature of these spectra is because we represent strain spectra as discrete modes rather than continuous wavenumbers.) This paper is concerned with the high-wavenumber portion of the slope spectra (labeled KMII above).

aspect ratios on the order of 100:1 (Rosenblum and Marmorino 1990). Here, similar spectra are related to directly measured turbulence dissipation rates. We are also able to examine the spectra in light of the intervening decades of internal wave and turbulence measurements, predominantly from vertical profilers.

Turbulence is usually measured from specialized vertical profilers (Osborn and Crawford 1980; Moum et al. 1995) or, more infrequently, horizontal towed instruments (Osborn and Lueck 1985; Fleury and Lueck 1992; Moum et al. 2002). Turbulence dissipation rate, ε, can be estimated using shear probes or from dissipation of temperature using fast thermistors. Shear probes are prone to vibration (Moum and Lueck 1985; Levine and Lueck 1999), requiring great care in instrument design and deployment. Thus most of this effort has gone into vertical profilers. Thermistors have a finite time constant that attenuates their signal at wavelengths that are relatively low for resolving turbulence (depending on drop speed; Gregg 1999). Internal waves dominate vertical profiles at low wavenumbers. There is a very narrow range of resolved turbulence. More specialized sensors, such as thermocouples, can extend the range to higher wavenumbers (Nash et al. 1999), but these sensors are fragile and do not last long (yet) in oceanic deployments. Estimating turbulence using less-delicate instrumentation would increase our sampling of mixing in the ocean.

There are methods to indirectly estimate turbulence from routine velocity and density measurements. One method is to estimate the strength of the internal wave field using shear and stratification, then relate it to dissipation rate (Gregg 1989; Polzin et al. 1995; Gregg et al. 2003). This method relies on a fully developed internal wave spectrum and does not appear to work well in coastal waters and near topography (MacKinnon and Gregg 2003; Kunze et al. 2002). Another approach is to calculate the size of density overturns and assume that the potential energy in the overturn is dissipated in some fraction of a buoyancy period (Thorpe 1977; Dillon 1982; Moum 1996b). This method works well in highly turbulent flows, but has problems in strongly stratified flows where conductivity–temperature–density (CTD) probes cannot resolve overturns (Klymak and Gregg 2004) and in weak stratification where noise or salinity spiking induces spurious overturns (Galbraith and Kelley 1996; Johnson and Garrett 2004).

In this paper, the turbulence dissipation rate is estimated directly from temperature spectra obtained using the horizontally towed vehicle, Marlin, with the same technology used on vertical profilers. The influence of turbulence extends to much lower wavenumber in slope spectra than in strain spectra (Fig. 1b). One consequence is that estimates of turbulence dissipation rate are more readily made from spectral scaling so that this type of estimate could be obtained with a towed commercial thermistor.

We start with a brief review of the internal wave and turbulence subranges (section 2), followed by a discussion of Marlin and the experiment site on the Hawaiian Ridge (section 3). The observed spectra are presented in section 4. Next, the high-wavenumber portion of the spectra is fit to turbulence models, and it is shown that the intermediate scales are fit by adding turbulence and

internal wave fits made independently at the extremes of their subranges (section 5). The spectra are fit to determine the turbulence dissipation rate (section 6), and we show that the fit can be done for coarse wavenumbers with equally good effect (section 7). We finish with a short discussion of the possible meaning of adding spectra from two disparate types of motion and the observation that the turbulence subrange extends to such large horizontal subranges (section 8).

2. Internal wave and turbulence subranges

The temperature signal is converted to vertical displacements $\zeta = z(T_0) - T$, then taking the first derivative to yield isopycnal slope ζ_x (Part I). The equivalent quantity from vertical profiles is called the vertical "strain" ζ_z. Displacements remove low-frequency, small-amplitude motions of Marlin (Part I).

a. Internal wave subrange

Part I argues that low wavenumbers are relatively well modeled by

$$\phi_{\zeta_x}^{\mathrm{IW}}(k_x) \approx \phi_0 k_x^{-0.5}, \tag{1}$$

where ϕ_0 depends on the stratification, energy level, and frequency content of the internal wave field. The amplitude, ϕ_0, is only weakly coupled to the energy level because resolved horizontal wavenumbers are heavily influenced by the saturated part of the wave field. The power law of the horizontal spectrum, $k_x^{-0.5}$, is a convolution of the linear ($\sim k_z^0$) and saturated ($\sim k_z^{-1}$) subranges (Part I). The two subranges are not distinct in horizontal measurements because of the dispersion relation of a broadband frequency spectrum. We use Eq. (1) as a model in this paper for simplicity, but emphasize that it does not reflect physics of the wave field.

b. Turbulence subrange

The turbulence spectrum at high wavenumbers is usually written as a combination of subranges. At the lowest turbulence wavenumbers, the strength of turbulence and the temperature gradient set the level of the displacement spectrum of the *inertial–convective subrange*:

$$\phi_{\zeta_x}^{\mathrm{IC}} = 2\pi\chi_\zeta C_T \varepsilon^{-1/3}(2\pi k_x)^{1/3} \quad [\mathrm{cpm}^{-1}], \tag{2}$$

where k_x is the horizontal wavenumber in cycles per meter, with $C_T \approx 0.4$ (Sreenivasan 1996), and ε is the turbulence dissipation rate. Here $\chi_\zeta = \chi_T(dT_0/dz)^{-2}$ is a scaled version of the dissipation of temperature variance χ_T, where dT_0/dz is the background temperature gradient. At higher wavenumbers, the viscosity of seawater (ν) becomes important in the *inertial–diffusive subrange*:

$$\phi_{\zeta_x}^{\mathrm{ID}} = 2\pi\chi_\zeta q \nu^{1/2}\varepsilon^{-1/2}(2\pi k_x), \tag{3}$$

where q is an empirical constant. In this paper we add the subranges to get

$$\phi_{\zeta_x}^{\mathrm{Turb}} = 2\pi\chi_\zeta[C_T\varepsilon^{-1/3}(2\pi k_x)^{1/3} + q\nu^{1/2}\varepsilon^{-1/2}(2\pi k_x)]. \tag{4}$$

Adding the subranges like this gives a value for q of 2.3, which is somewhat lower than is used by other investigators. This difference is the subject of ongoing research but does not affect the results reported here.

At the highest wavenumbers there is a viscous–diffusive subrange that is not discussed further here.

To relate the spectra to ε, the dependence on χ_ζ is removed as follows. The temperature variance dissipation rate is

$$\chi_T = 2D_T\langle(\nabla T)^2\rangle, \tag{5}$$

where D_T is the molecular diffusivity of water and the angle brackets represent averaging over a homogeneous turbulent patch. Ignoring the lateral and time-dependent terms, the turbulent equation for temperature variance can be written:

$$D_T\langle(\nabla T)^2\rangle = -\langle w'\,T'\rangle\frac{\partial T}{\partial z} \tag{6}$$

$$= K_T\left(\frac{\partial T}{\partial z}\right)^2, \tag{7}$$

where the turbulent temperature flux $\langle w'\,T'\rangle$ has been cast as a Fickian diffusion working against the mean temperature gradient. These equations can be combined to yield

$$\chi_T = 2K_T\left(\frac{\partial T}{\partial z}\right)^2. \tag{8}$$

If turbulent motions affect buoyancy in the same way they do temperature, $K_\rho = K_T$: K_ρ is routinely linked to the turbulence dissipation rate and stratification via the Osborn method,

$$K_\rho = \Gamma\frac{\varepsilon}{N^2}, \tag{9}$$

where $\Gamma \approx 0.2$ is an empirically defined mixing efficiency (Osborn and Cox 1972; Osborn 1980; Moum 1990, 1996a). This gives

$$\chi_T = 2\frac{\Gamma\varepsilon}{N^2}\left(\frac{\partial T}{\partial z}\right)^2. \quad (10)$$

Vertical displacement gradients can be approximated by dividing the spectra by $(dT_0/dz)^2$. Assuming that, on average, $\partial T/\partial z \approx dT_0/dz$, and approximating N^2 by the mean N_0^2:

$$\chi_\zeta = 2\frac{\Gamma\varepsilon}{N_0^2}, \quad (11)$$

Eq. (4) is rewritten as

$$\phi_{\zeta_x}^{\text{Turb}}(k_x) = 4\pi\frac{\Gamma\varepsilon}{N_0^2}[C_T\varepsilon^{-1/3}(2\pi k_x)^{1/3} + q\nu^{1/2}\varepsilon^{-1/2}(2\pi k_x)] \quad [\text{cpm}^{-1}]. \quad (12)$$

Using the mean rather than the local gradients is a necessary approximation when using a towed instrument. If N^2 is proportional to $\partial T/\partial z$, as it is in the limited depth ranges considered near Hawaii, then the error in performing the approximation is linear in N^2. The model will underestimate the spectra where $N_0^2 > N^2$. In the fits performed below this means that ε will be overestimated in regions of high strain.

c. Intermediate subranges

The wavenumbers between turbulence and internal waves have engendered considerable attention because no appropriate theory exists for the motions there. With horizontal gradient spectra similar to those presented here, McKean and Ewart (1974) note that wavenumbers between internal waves and turbulence had an almost white subrange. McKean (1974) makes a case that the whitening is due to the vertical advection of finescale motions past the instrument. However, his model of turbulence did not include an inertial subrange. The slope of the inertial subrange, $k_x^{1/3}$, is relatively white and accounts for much of the whitening. We will demonstrate below that any remaining whitening of the spectrum at midwavenumbers can be accounted for by summing the turbulent and internal wave spectra:

$$\phi = \phi^{\text{IW}} + \phi^{\text{Turb}}. \quad (13)$$

3. Instrumentation and experiment site

Marlin is a towed vehicle, described in Moum et al. (2002), Klymak et al. (2006), and Part I. A 0.680-in. hydrographic wire deployed from the deck is weighted with a streamlined 1500-kg depressor. Marlin is attached to the depressor via a 200-m-long cable with strain relief to damp any remaining vibration. Marlin was ballasted to fly between 20 and 50 m below the depressor. Tow speeds were approximately 1 m s^{-1} with variations in the speed and currents inducing small speed and altitude variations in Marlin, though the cable and depressor damped out ship motions shorter than 20 min. Marlin was equipped with a microstructure suite and conductivity, temperature, and pressure on the nose, and a temperature sensor on a fin that protruded 1.16 m beneath the body (Part I).

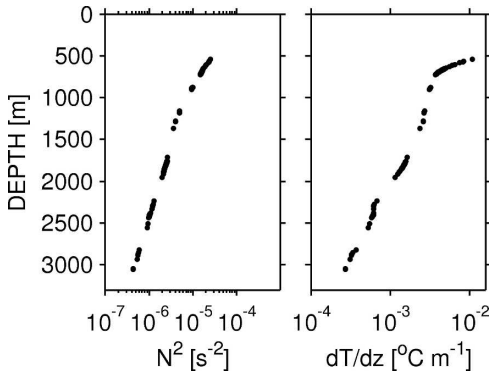

FIG. 2. (a) Mean stratification profiles for spectra used in this paper. (b) Mean temperature gradient profiles. Each dot corresponds to an individual spectra. Profiles were derived from vertical measurements made during the same experiment (Lee et al. 2006).

The data in this paper were collected from Kauai Channel between Oahu and Kauai as part of the Hawaii Ocean Mixing Experiment (HOME). Our sampling consisted of cross-ridge runs made at approximately 700-m depth and a dogleg pattern of runs that approached the ridge, then turned northwest, following the 3000-m isobath (Klymak et al. 2006). Most of the data presented in this paper were collected near 700 m. At this depth, the mean vertical stratification was $N^2 = 2 \times 10^{-5}$ s^{-2}; the vertical temperature gradient $dT/dz = 4 \times 10^{-3}$ °C m^{-1} (Fig. 2).

The microstructure suite includes airfoil probes from which estimates of ε are obtained by standard methods (Moum et al. 1995). Contamination of ε measurements by vehicle vibration were diagnosed using accelerometers in the nose of the microstructure package (Levine and Lueck 1999). Vibration signals coherent with the shear probe signals were removed from the signals and the variance computed to get the dissipation rate. If more than one-half of the variance was removed, the calculated dissipation rate was assumed to be dominated by noise and set to $\varepsilon = 10^{-11}$ m^2 s^{-3}. This biases

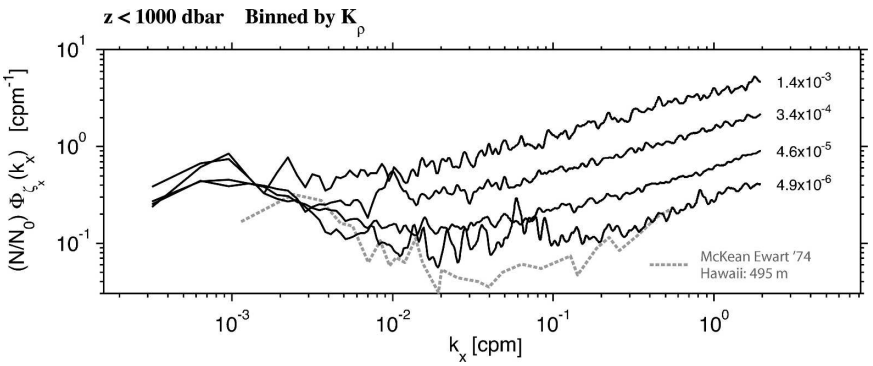

FIG. 3. Average isopycnal slope spectra, binned in one-decade bins of the turbulent diffusivity (as estimated from the shear probes). Spectra have been normalized by their buoyancy frequency for comparison with other studies (though this will not normalize the high wavenumbers). Dashed line is a spectrum from McKean and Ewart (1974, their Fig. 2a), collected farther offshore at 495-m depth at Hawaii.

dissipation averages low, but has minor effect as the signal-to-noise level increases (Moum et al. 2002). For the data discussed here, the noise level was $O(\varepsilon \approx 3 \times 10^{-10}\ \mathrm{m^2\ s^{-3}})$.

4. Isopycnal slope spectra

Isopycnal slope spectra on wavelengths of 5 km to 0.1 m are presented in the companion paper, Part I. We convert temperature to vertical displacements using the background temperature gradient and take the derivative in the along-measurement direction to get isopycnal slopes. Binning these spectra by turbulence intensity reveals a systematic variation to the spectra (Fig. 3). The 5-km spectra are binned by $K_\rho = 0.2\varepsilon/N^2$, which can be considered a dissipation anomaly, where $K_\rho = 10^{-5}\ \mathrm{m^2\ s^{-1}}$ is the open-ocean background. The amplitude of the spectra are normalized by N/N_0 ($N_0 = 5.3 \times 10^{-3}\ \mathrm{s^{-1}}$) after the Wentzel–Kramers–Brillouin scaling (Katz and Briscoe 1979), though N only varies by a factor of 2 for the spectra replotted here (Fig. 2a). Binning demonstrates how the spectra vary with dissipation rate.

At low wavenumbers, the spectra almost collapse. In Part I, we interpret the low-wavenumber part of the spectrum as internal waves. At high wavenumbers, the spectra have increasing amplitude with increasing ε. This increase, and a blue slope, extends down to wavenumbers $k_x \lesssim 10^{-2}$ cpm for all but the weakest turbulence bin.

5. Interpreting turbulence in the presence of internal waves

The averaged isopycnal slope spectra remain slightly blue, even to wavenumbers $k_x < 10^{-2}$ (Fig. 3). Part I shows that the crossover where the fit to turbulence dominates the internal wave fit varies inversely with turbulence dissipation rate. This section demonstrates that these motions have spectral shapes and vertical coherence consistent with turbulence. We also show that the shape of spectra between the two types of motion is fit by a linear addition of the models.

a. Goodness of fit

A complete model for the slope spectra includes internal wave, inertial–convective, and inertial–diffusive subranges:

$$\tilde{\phi}_{\zeta_x}(k_x) = \phi_0 k_x^{-0.5} + 4\pi \frac{\Gamma\varepsilon}{N_0^2}[C_T\varepsilon^{-1/3}(2\pi k)^{1/3} + q\nu^{1/2}\varepsilon^{-1/2}(2\pi k)]. \quad (14)$$

The internal wave amplitude ϕ_0 is fit over wavenumbers where there is a distinct red spectrum, or to $k_x = 10^{-2}$ cpm. Three examples show the procedure (Fig. 4) where the low- and high-wavenumber fits are indicated as well as the sum of the two. Turbulent wavenumbers are fit by varying ε to minimize

$$e = \int_{k_0}^{k_+} [\log 10(\phi^{\mathrm{Turb}}/\phi')]^2\, dk \quad (15)$$

with $k_0 = 0.4$ and $k_+ = 4$ cpm. The two fits are carried out sequentially: the turbulent fit first, then the internal wave fit, since the low wavenumbers are sometimes dominated by turbulence. In neither case are the spectra fit between $10^{-2} < k_x < 0.4$ cpm, outside the range of ambiguity between internal waves and turbulence.

Despite being fit over limited subranges, the model does well over intermediate wavenumbers as well (Fig. 4). The logarithmic mean of $\phi/\tilde{\phi}$ as a function of wavenumber rises slightly and then dips at the lowest wave-

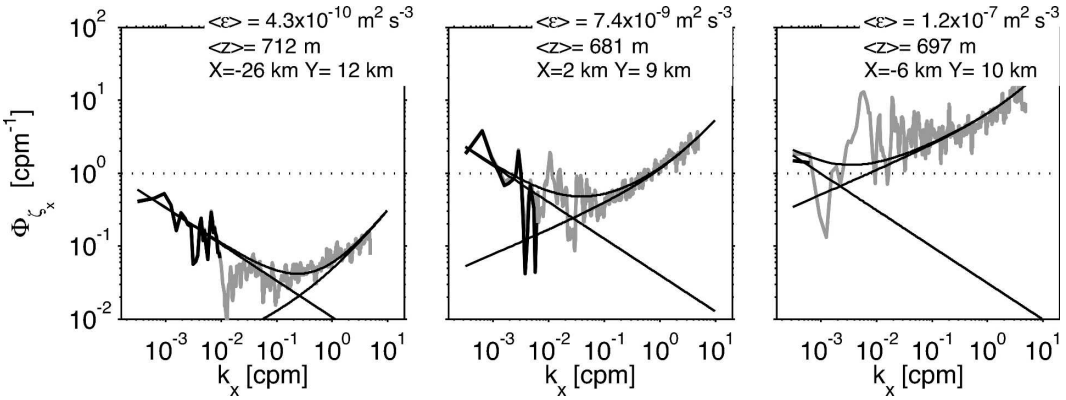

FIG. 4. Example spectral fits showing the low- and high-wavenumber fits. Low wavenumbers are fit only in the region of the spectra in solid black, either $k_x < 10^{-2}$ cpm or to the wavenumbers where the turbulence fit dominates the spectrum; (right) only the lowest two wavenumber bins are fit. The high spectrum is fit from $0.4 < k_x < 4$ cpm.

numbers, exhibiting some curvature over the turbulence range of the fit (Fig. 5). The average misfits are less than a factor of 2 and, in most cases, are not statistically significant. The dip at intermediate scales ($k_x \approx 10^{-2}$ cpm) may indicate that the turbulence model is too aggressive at these wavenumbers, and turbulence is starting to roll off.

b. Coherence between nose and fin

The shape of the spectra agree well with the model. However, being able to match spectral shapes does not necessarily mean signals are governed by the physics associated with each subrange. The coherence between two vertically separated sensors provides additional information. The coherence of signals from the nose on Marlin and a fin below the nose demonstrate that the coherence is a linear combination of what we are calling "turbulence" with what we are calling "internal waves."

A temperature sensor was installed on the fin 1.16 m below and 1.9 m behind the nose. There were two cross-ridge tows (approximately 150 km total) at $z \approx 700$ m where the fin thermistor was calibrated and used for coherence estimates. For all data, the coherence at $k_x =$

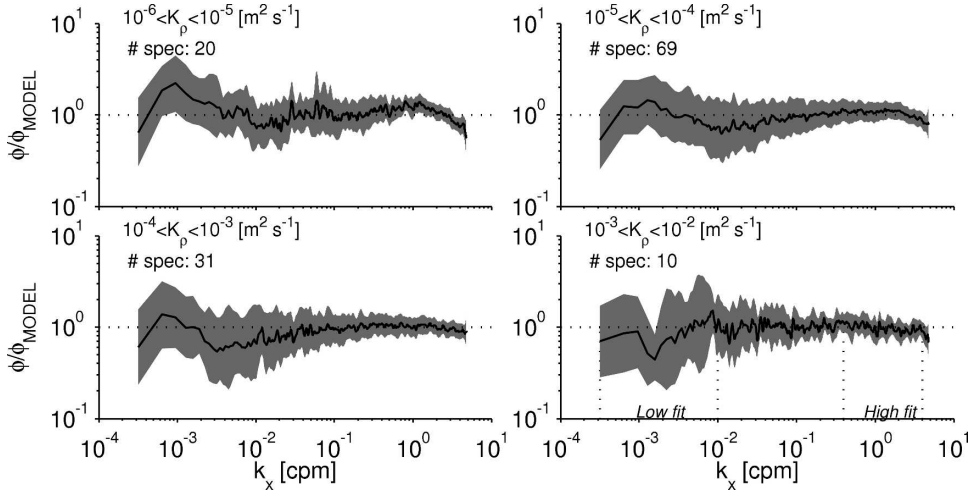

FIG. 5. Dissipation-binned spectra divided by the model fit [$\tilde{\phi}$, Eq. (14)]. Shading represents half a standard deviation assuming a lognormal deviation of the ratios. Smoothing of the errors in logarithmic bins of wavenumber space reduces the standard deviations at high wavenumbers. (lower right) Dashed lines indicate regions of the respective fits. Note that the low wavenumbers are fit after the high-wavenumber model has been subtracted from the spectra. This can mean that the model at the low wavenumbers is entirely dominated by the turbulence. In the lower-right panel this makes the mean misfit drop below unity.

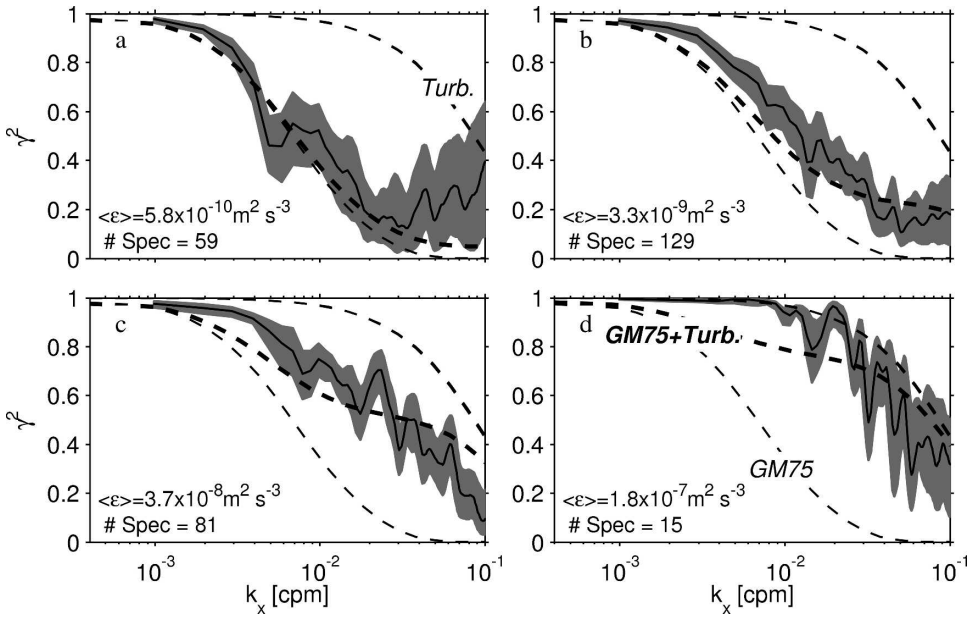

FIG. 6. Towed vertical coherence (squared) between Marlin's nose and a fin 1.16 m below and 1.9 m behind the nose. Data are averaged in four turbulence bins, and 95% bootstrap confidence intervals are made for each wavenumber. The lower thin dashed line is the vertical coherence expected from the GM75 spectrum (with bandwidth parameter $j_* = 1$, Part I), the upper thin dashed line is the coherence expected from homogeneous, isotropic turbulence. The middle thick dashed line is the coherence expected from a temperature field that is a linear combination of the two types of motion.

10^{-3} cpm approaches unity (Fig. 6). To compare with theory, the fin sensor was lagged by 1.9 m.

Binning the coherence between the two sensors by ε shows that, as ε increases, the observed coherence between the two sensors rises (Fig. 6). At the lowest dissipation rates, the coherence rolls off at $k_x \approx 3 \times 10^{-3}$ cpm, indicating that the motions have a low aspect ratio. As ε increases, the coherence increases, and for the largest ε the roll off is near $k_x \approx 4 \times 10^{-2}$ cpm (Fig. 6d).

We model this increase of coherence at high wavenumbers by calculating the coherence based on modeled spectra of the motion. The coherence between two sensors vertically separated by Δz can be calculated from a model spectrum of the motion $\phi(k_x, k_y, k_z)$ as

$$\gamma = \frac{\int\int \cos(k_z \Delta z)\phi(k_x, k_y, k_z)\, dk_y\, dk_z}{\phi(k_x)}. \qquad (16)$$

For the motions considered here, $\phi(k_x, k_y, k_z) = \phi^{\mathrm{IW}}(k_x, k_y, k_z) + \phi^{\mathrm{Turb}}(k_x, k_y, k_z)$. The combined coherence is simply the weighted sum of the coherences of the components:

$$\gamma = \frac{\gamma^{\mathrm{IW}}\phi^{\mathrm{IW}} + \gamma^{\mathrm{Turb}}\phi^{\mathrm{Turb}}}{\phi^{\mathrm{IW}} + \phi^{\mathrm{Turb}}}. \qquad (17)$$

The procedure for calculating γ^{IW} is given in Katz and Briscoe (1979). For the GM75 model spectrum, γ^{IW} yields the lower thin dashed lines in Fig. 6. In the bin with the lowest turbulence (Fig. 6a), the observed coherence is consistent with the GM75 coherence, indicating that the motions are dominated by internal waves.

The vertical coherence of the turbulence part of the motion, γ^{Turb}, can be calculated in a similar manner. We could not find a reference for this, so we derive the coherence here. We infer $\phi^{\mathrm{Turb}}(k_x, k_y, k_z)$ from the one-dimensional spectrum $\phi_\zeta^{\mathrm{Turb}}(k_x)$ [Eq. (12) divided by $(2\pi k_x)^2$] using the assumption that the turbulence is isotropic (Tennekes and Lumley 1972, p. 281):

$$\phi^{\mathrm{Turb}}(K) = -\frac{1}{2\pi K}\frac{d}{dK}\phi_\zeta(K), \qquad (18)$$

where $K = (k_x^2 + k_y^2 + k_z^2)^{1/2}$. Substituting K for k_x in Eq. (12) gives

$$\phi^{\mathrm{Turb}}(K) = \frac{4\pi\Gamma\varepsilon}{4\pi^2 N^2}\left[\frac{5}{3}C_T\varepsilon^{-1/3}(2\pi K)^{-11/3} + q\nu^{1/2}\varepsilon^{-1/2}(2\pi K)^{-3}\right]. \qquad (19)$$

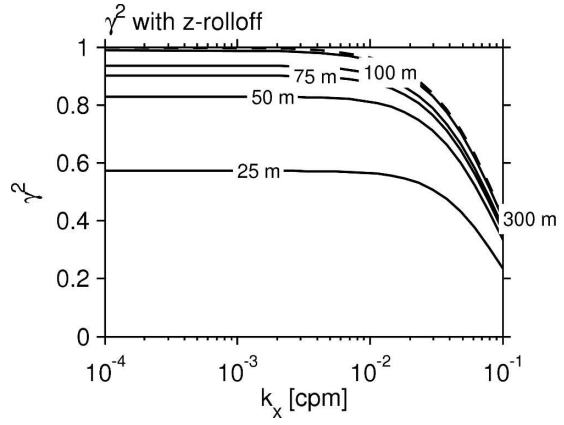

FIG. 7. Effect on the vertical coherence of 1.16-m separated sensors of attenuating the three-dimensional turbulence in the vertical at the scale indicated for each line. This is a crude approximation to anisotropic turbulence. The dashed line is for no attenuation.

We calculate $\gamma^{\text{Turb}}(k_x)$ numerically using Eq. (16) to yield the upper dashed curve in Figs. 6a–d. The coherence of a turbulent field is higher than the coherence of internal waves at all wavenumbers and only begins to fall off at $k_x > 0.03$ cpm. When ε is highest, observed coherences (Fig. 6d) are close to the purely turbulent model.

The weighted sum of the internal wave and turbulence coherences is the thick dashed line in each panel (Figs. 6). We have assumed that ϕ^{IW} remains constant, as indicated by Fig. 3, and increased ϕ^{Turb} in each panel. As ϕ^{Turb} increases, the increase and the shape of the increase in coherence is predicted. The observed coherence tends to be a little higher than the model predicts for all dissipation levels, particularly for the highest dissipation bin.

This calculation assumes a simple addition of turbulence and internal wave spectra, just as we did above in fitting the shape of the spectra. Neither the fits nor these coherence calculations are perfect. However, they explain the leading-order features of the spectra without the need for additional physics and indicate that the signature of turbulence extends to wavenumbers $k_x < 10^{-2}$ cpm.

A caveat is that we have assumed for simplicity that the turbulence spectrum exists and is isotropic at all wavenumbers. However, turbulence is thought to be driven by the overturning of shear or convective instabilities, which have finite vertical extents, so this assumption is not likely to hold at large vertical scales (Gargett 1985). The effect of anisotropy can be estimated by attenuating $\phi^{\text{Turb}}(K)$ at large vertical scales (Fig. 7). This is only a crude approximation of anisotropy but, in lieu of a complete theory, we assess the possible effect on our measurements. Attenuating the spectra at a 100-m scale, the coherence is nearly the same as for the fully isotropic case. However, if turbulence is suppressed at smaller scales, the coherence starts to drop significantly. This argues that the coherence from the most turbulent blocks of data (Fig. 6d) consists of turbulence that extends to vertical scales in excess of 100 m. Other work at the study site corroborates the idea that the strongest turbulence is contained in turbulent patches of greater than 100 m in height. Averages from weaker turbulence blocks are not definitive and could be consistent with the turbulence being suppressed in the vertical at smaller scales.

6. Calculating the dissipation rate from thermistors

In this section we consider how well the dissipation rate can be estimated from the turbulence portion of the temperature spectrum. We consider 32-m-long sections of data, yielding approximately 9000 spectra. This scale was chosen as being free of contamination from internal waves for most of the observations (Part I, their Fig. 10). Average turbulence dissipation ε was estimated with shear probes over the same intervals to compare with the value estimated from the thermistors (ε_T).

We obtain ε_T as the value of the dissipation that minimizes Eq. (15) over $0.4 < k_x < 4$ cpm. Again, the cruise-background stratification is used to estimate N^2. Fitting temperature spectra to obtain ε_T yields encouraging results (Fig. 8). There is considerable spread in the estimates, and individual 32-m blocks of data may make an incorrect estimate by over an order of magnitude but the average results are unbiased. Contributing to the scatter in this comparison is our inability to determine the local value of N^2, as well as natural geophysical variability.

Spatial binning of ε_T across the ridge shallower than 1000 m demonstrates that the temperature sensors replicate the cross-ridge structure observed with shear probes (Fig. 9). The dissipation estimate from the temperature sensor was first smoothed on a 300-m scale in log space to remove some of the lognormal variability, equivalent to averaging 10 spectra before performing the fit. Both estimates of turbulence dissipation were then binned arithmetically in 5-km bins. There is good agreement across the ridge except on the northernmost edge, where there is not as much data.

As mentioned above, a major drawback of this analysis is not having reliable local values of the stratification N^2. We could have formed stratification estimates from the fin sensor and another body towed ~40 m above and ~200 m in front of Marlin but the second body was

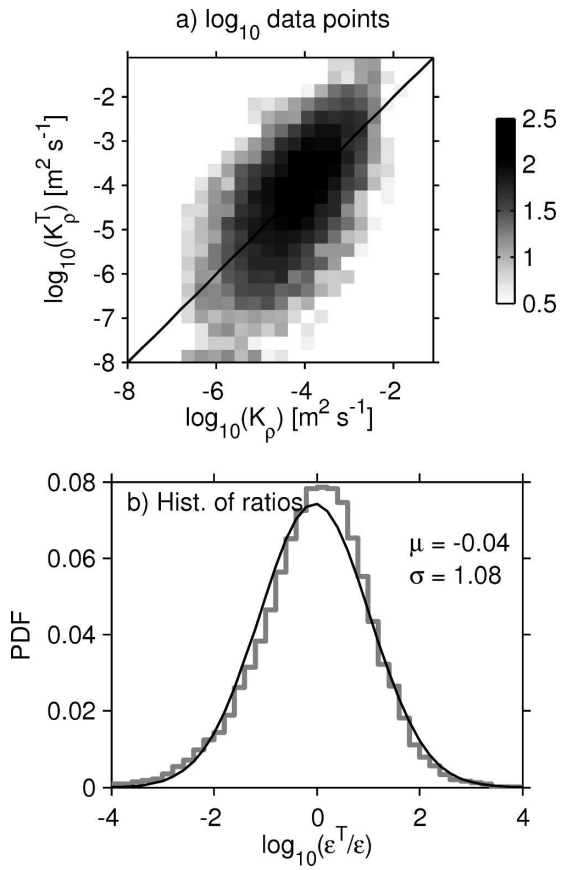

FIG. 8. Comparison of $K_\rho^T = 0.2\varepsilon_T N^{-2}$ estimated from 9059 displacement spectra and from the shear probes. (a) Two-dimensional histogram of the two estimates. The correlation coefficient between the two estimates is $r = 0.56 \pm 0.01$. (b) Histogram of the log of the ratios. The lognormal statistics (mean, μ, and standard deviation, σ, of a Gaussian fit) of the log of the ratio are shown.

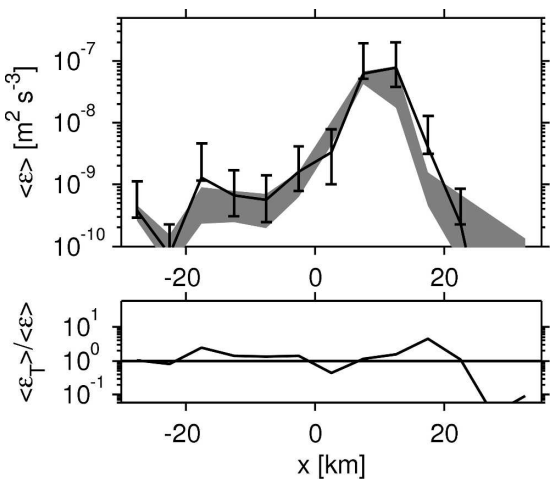

FIG. 9. Dissipation from the shear probes (gray shading) and from the temperature spectra (line and error bars). Error bars represent bootstrap means in 5-km spatial bins. The crest of the ridge is from approximately 10 to 20 km (see Klymak et al. 2006).

felt to be too far from Marlin to be useful, and at an aspect ratio that could confuse isopycnal slopes with stratification estimates. The fin was too close to the nose and in turbulent flows was just as likely to be measuring part of an overturn than not. The magnitude of the temperature gradient across any two points in an overturn is likely to be greater than the mean temperature gradient across the whole overturn. The usual approach with vertical profilers is to sort the density first, alleviating this problem, and arriving at a useful measure of stratification but this cannot be done with two-point sensors.

The uncertainty in N^2 increases the spread in the distribution between the two estimates. The disagreement will also have a bias if there is a correlation between N^2 and ε. There is evidence that lower than normal N^2 increases the likelihood of turbulence in the open ocean (Alford and Pinkel 2000), a result that appears applicable near topography at Hawaii (Levine and Boyd 2006; Aucan et al. 2006). This will bias our temperature spectra dissipation estimates slightly high (Fig. 9).

We have also assumed that the mixing efficiency, Γ, is a constant. There is evidence that Γ may depend on the buoyancy Reynolds number (Smyth et al. 2001) and thus ε and N^2, possibly biasing our estimates. This dataset is not adequate to test this possibility.

7. Resolution requirements

The ability to see further into the inertial–convective subrange with horizontal tows than vertical profiles opens the possibility of using less-specialized vehicles and sensors to determine turbulence dissipation rates in the ocean. As an example, the temperature probe on a Seabird 9-11 CTD has a noise level of 2×10^{-4} °C at 24 Hz. The frequency response of these sensors is limited by the rate that temperature can diffuse through the protective coating to the thermistor, and attenuates near 8 Hz (Gregg and Meagher 1980). These effects limit the upper wavenumber at which turbulence can be seen with a commercial sensor. As shown here, the lower wavenumber is a function of the relative strength of the internal wave band and turbulence.

We explore the feasibility of using a lower-resolution temperature sensor to fit temperature spectra from a towed vehicle by plotting the isopycnal slope spectrum for three depths and for a slow (like Marlin, 1 m s^{-1}) and moderate (like SeaSoar, 4 m s^{-1}) tow speed (Fig. 10). At the slow tow speed, there is no issue with noise

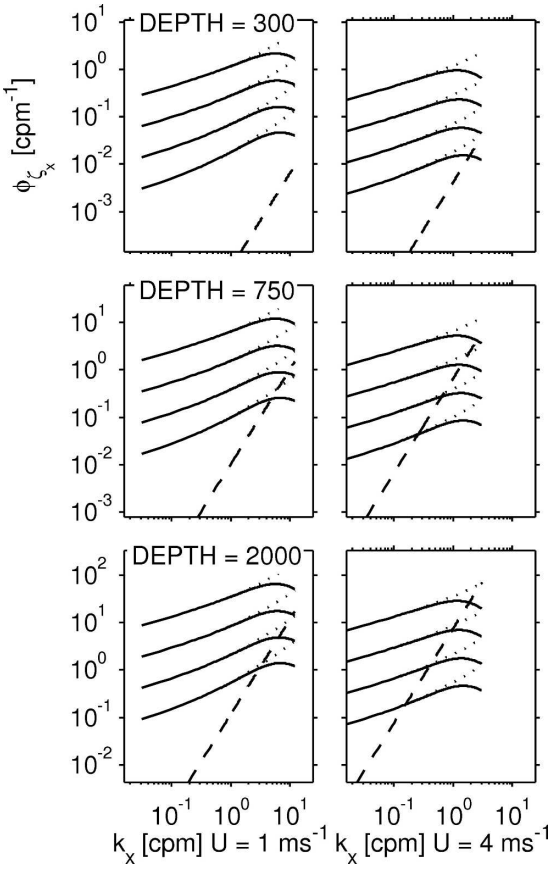

FIG. 10. (left column) Theoretical isopycnal slope spectra for an instrument towed at 1 m s^{-1} at three different depths (i.e., stratifications and temperature gradients); (right column) tows at 4 m s^{-1}. Dotted lines are the theoretical displacement spectra for four decades of turbulent diffusivity (starting at $K_\rho = 3 \times 10^{-6}$ m^2 s^{-1}). Black lines include an approximate response expected for a temperature sensor with a roll off at 8 Hz. Dashed lines are the noise floor of an instrument with 2×10^{-4} °C noise at 24-Hz sampling rate.

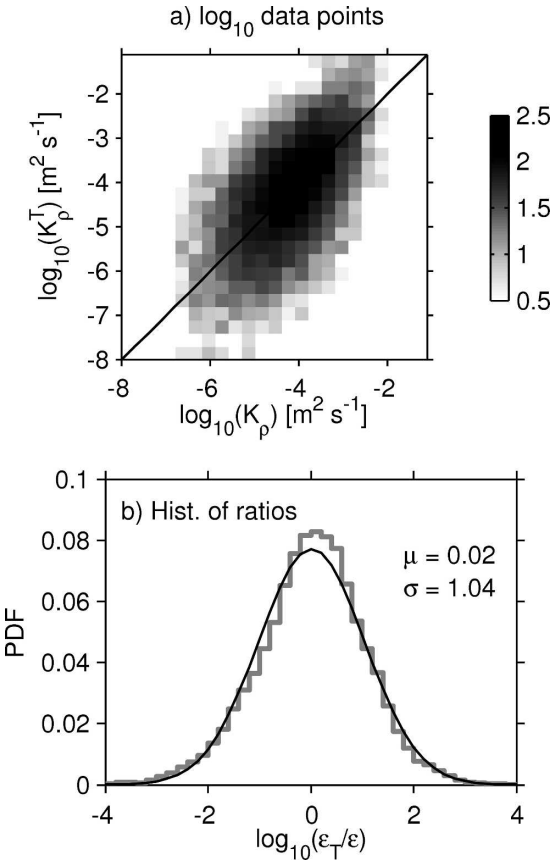

FIG. 11. As in Fig. 8 except the fit to ε_T was made on the displacement spectra for low wavenumbers $0.04 < k_x < 0.4$ cpm, a wavelength well within the range of CTD with a 3-Hz roll off moving at 4 m s^{-1}. The correlation between the two estimates did not change.

except for the weakest dissipations at the deepest depths. At faster tow speeds, the wavenumber bandwidth of the measurements is reduced and measurement noise level becomes a factor. However, in much of the ocean large dissipation rates should be detected via this method.

We test this by subsampling our data to represent a more poorly resolved measurement of temperature. Displacement spectra were fit in the wavenumber range $0.04 < k_x < 0.4$ cpm (reducing scales by a factor of 10 compared to our estimates of ε_T). While this would probably not work for weak turbulence at 2000 m and a speed of $U = 4$ m s^{-1}, it should be adequate at 700 m. The estimates at these lower wavenumbers are not statistically different from those between $0.4 < k_x < 4$ cpm (Fig. 11).

8. Summary and discussion

This paper describes turbulence temperature spectra from a horizontally towed platform in stratified waters near a site of intense internal wave generation. These results are unique because the data were collected in an environment with turbulence levels spanning the highest seen in noncoastal waters to the quiet open ocean. This is also the first time that direct turbulence measurements have been coupled with thermistors for horizontal deep-water tows.

These results have yielded the following insights into isopycnal slope spectra:

1) Horizontal spectra exhibit a turbulence shape ($\phi_{\zeta_x} \sim k_x^{1/3}$) to surprisingly low wavenumbers;
2) The subrange between the internal-wave-dominated wavenumbers and the turbulence-dominated wavenumbers is modeled by the linear addition of spectral amplitude;

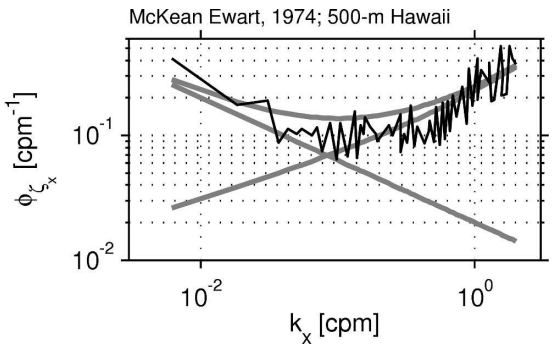

FIG. 12. Fit of the spectrum from McKean and Ewart (1974, their Fig. 2c), 500 m (also note that their spectra are half spectra, so we have multiplied by 2). The dissipation rate fit to the model is $\varepsilon = 1.9 \times 10^{-9}$ m^2 s^{-3}, or $K_\rho = 1.4 \times 10^{-5}$ m^2 s^{-1}. For this plot $dT/dz = 6 \times 10^{-3}$ °C m^{-1}, and $N = 5.2 \times 10^{-3}$ s^{-1}. The spectrum was digitized from their paper by hand.

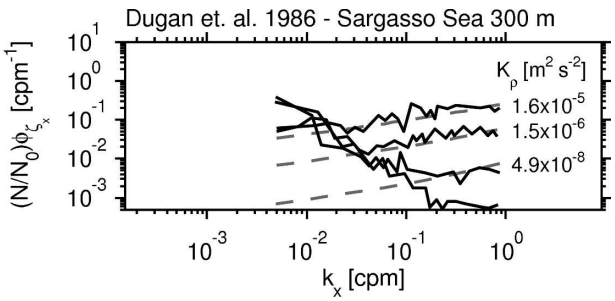

FIG. 13. Spectra digitized from Dugan et al. (1986, their Fig. 3). Spectra are binned by the authors as "patches of varying intensity." These have been whitened and scaled as in this paper, $dT/dz = 0.11$°C m^{-1} and $N = 1.8 \times 10^{-2}$ s^{-1}. Turbulence subrange was fit for ε (dashed lines), expressed as K_ρ. Note that the highest values of K_ρ here are comparable to the lowest in this paper.

3) ε can be reasonably estimated from these spectra by an inverse of the Osborn method, even with measurements that can resolve only scales larger than a few meters.

The last observation is useful as an alternate way to estimate turbulence dissipation in the ocean using relatively inexpensive instrumentation. It is important to make the distinction between slope and strain spectra, where internal waves intersect the turbulence spectra at $k_x \approx 1$ cpm (Fig. 1a). Because of the limited wavenumber range of turbulence in the strain spectra, extraction of meaningful estimates of ε is impossible without specialized sensors.

The first two observations bring up interesting questions about the nature of turbulence at large horizontal scales.

a. Why add the spectra?

We have fit the internal wave and turbulence subranges at wavenumbers where they do not contaminate one another. Simply adding spectral amplitudes, fit at these extrema, provides a reasonable fit to the spectra at intermediate wavenumbers (Fig. 5). Simple addition of the spectral models also does a good job of predicting the coherence between two vertically separated sensors (Fig. 6). In neither case, however, does the model perfectly fit the data, so it is possible to conceive of other physics than what we have proposed here. However, this additive model has the benefit of simplicity.

We have no a priori justification for adding the spectra in this way. Typically a sharp change between the subranges is used (but also not usually tested). Perhaps a combination of two factors is responsible for the agreement. First, turbulence is observably intermittent over 5-km spectra, so at any given wavenumber the dominant physics is sometimes turbulence and sometimes internal waves. We have made no attempt to consider homogeneous "patches" of turbulence, primarily because it would be hard to do so and still present internal wave spectra. Second, there is no reason that "turbulence" cannot coexist with internal waves. We expect this additive model applies to vertical spectra as well, but the sharper slope of the internal wave spectra (k_z^{-1} versus $k_x^{-0.5}$) means that the region of overlap is less pronounced. For now, we present the additive model as an observation and hope that an explanation can be refined from laboratory, numerical, and further field work.

b. Why does the turbulence shape extend to such low wavenumbers?

A related issue is the low-wavenumber extent of the turbulence. For the most intense turbulence, there is evidence of a $\phi_{\zeta_x} \sim k_x^{1/3}$ turbulence subrange influencing the spectra to scales exceeding 500 m.

The results in this paper are similar to those of other authors, so we believe that the low-wavenumber extent of the $k^{1/3}$ inertial subrange is not isolated to our measurements. A spectrum from McKean and Ewart (1974, their Fig. 2a) is shown in Fig. 3. This spectrum increases and becomes blue at high wavenumbers. Another of their spectra (Fig. 2c, their paper) is fit in Fig. 12. Note that the fit is satisfactory at the wavenumbers between the subranges, reducing the need for the additional physics as proposed by McKean (1974).

The results reported by Dugan et al. (1986) are also similar to those presented here (Fig. 13). They measured horizontal temperature spectra in the Sargasso Sea, which they binned by the "intensity" of patches. This yielded spectra that are largely collapsed at low

wavenumbers but have varying levels at wavenumbers $k_x > 2 \times 10^{-2}$ cpm. As they note, the slope in this regime is consistent with an inertial subrange, particularly for the two most turbulent spectra. The results of this paper corroborate these results and verify that increasing intensity corresponds to increasing turbulence dissipation levels. Here we estimate the turbulence dissipations from their data and find very low numbers, consistent with vertical microstructure measurements that also find low dissipation in the Sargasso Sea (Gregg and Sanford 1980). These are further evidence that the inertial subrange can extend to large horizontal scales. In this case, the largest scales are about 50 m, comparable with the weakest dissipation spectra in Fig. 3 and much larger than any overturns that would be found in such stratified water (even at 1000 times the background dissipation rate, the Ozmidov scale is only $L_0 = 0.5$ m).

It seems unlikely that motions in our data at $k_x < 10^{-2}$ cpm are isotropic turbulence. The large turbulence patches are probably associated with large breaking waves near the ridge, similar to those found on the flanks (Levine and Boyd 2006; Aucan et al. 2006), but these were not observed to exceed 150 m on top of the ridge at the depths discussed here and were usually O(50 m). Therefore, the motions at these intermediate wavenumbers are anisotropic.

The horizontal extent of turbulence patches is poorly understood. Turbulence structures in Hawaii can be observed at a single mooring for a number of hours, and Marlin is towed through patches of elevated turbulence that are several kilometers long (Part I, Fig. 5), indicating that turbulence patches have a large aspect ratio. Similar results have been observed elsewhere. Itsweire et al. (1989) found 10-m-thick layers of unstable Richardson number extending over several kilometers in the upper 100 m of the ocean. Marmorino (1987) discusses a 3-km-long patch that has evidence of active turbulence from a temperatures sensor. The aspect ratio of turbulence patches has been argued to be f/N, where f is the Coriolis frequency (Rosenblum and Marmorino 1990). At 700 m at Hawaii $f/N = 0.01$, so a 10-m-thick patch could conceivably be 1 km long. Numerical modeling (Smyth et al. 2001) and oceanic observations (Seim and Gregg 1997; Moum et al. 2003) indicate that turbulence created by Kelvin–Helmholtz billows has a flattened aspect ratio, and it seems reasonable that the same will be true of convective instabilities.

We are not aware of numerical or laboratory studies that have ascertained the form for horizontal spectra of turbulence beyond the vertical scale of the patch. Therefore, we have no theoretical explanation for extending the inertial subrange to such large horizontal scales. Most numerical experiments are limited in horizontal extent to contain only one or two overturning scales (Smyth et al. 2001). Numerical work by Riley and deBruynKops (2003) and Lindborg (2006) indicates that turbulence can decay into a continuum of flattened vortices in the horizontal that appear to have a spectral slope similar to those discussed here. This "stratified turbulence" also has a vertical gradient spectra power law of k_z^{-1}, perhaps providing a framework to explain both the turbulence and the "saturated" subranges observed in vertical profiles. Our results indicate that the appropriate shape is a continuation of $\phi_{\zeta_x} \sim k_x^{1/3}$, until either the patch width is reached or the motions are dominated by internal waves. We hope that these observations spur further research into the nature of this anisotropic regime.

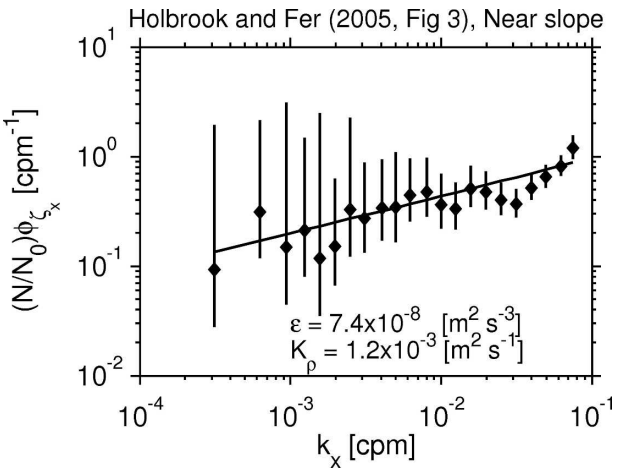

FIG. 14. Near-slope spectrum from Holbrook and Fer (2005). Data have been plotted assuming traces from their seismic image follow isopycnal displacements, ζ; $N = 3.5 \times 10^{-3}$ s^{-1} for the calculations made here. The fit was for $4 \times 10^{-3} < k_x < 2 \times 10^{-2}$ cpm.

Finally, Holbrook and Fer (2005) note that horizontal spectra computed from traces of seismic reflection transects near the continental rise show that spectra of the reflector displacement have $\phi_{\zeta_x} \sim k_x^{1/3}$ at $k_x < 10^{-2}$ cpm (Fig. 14). A fit to their data predicts a relatively large $K_\rho \approx 10^{-3}$ m^2 s^{-1}, though this value would fall in the third-highest dissipation bin used above (Fig. 3). The "open ocean" spectrum from their paper (not shown here) does not contain a distinct inertial subrange, but the spectral levels are low enough to suggest $K_\rho < 5 \times 10^{-5}$ m^2 s^{-1}. The spectrum in Fig. 14 demonstrates a slight dip at $k_x > 2 \times 10^{-2}$ cpm, which cannot be explained by our model, above which there is a noise floor ($\phi_{\zeta_x} \propto k_x^2$). Interpreting seismic data in terms of internal motions is still in its infancy, so the physical meaning of the spectra is still being investigated. However, the seismic results and those reported

here suggest that acoustics can possibly be used to remotely estimate strong turbulence dissipation rates.

Acknowledgments. Our thanks are given to the technicians of the Oregon State University (OSU) Ocean Mixing Group—Michael Neeley-Brown, Raymond Kreth, and Greig Thompson—whose hard work made these data possible. Thanks also are given to the captain and crew of the R/V *Wecoma* for their patience and skill in keeping Marlin flying on a straight path. Steven Holbrook and Ilker Fer kindly provided the data for Fig. 14. Valuable discussions were held with Bill Smyth, Rob Pinkel, Jennifer MacKinnon, Jim Riley, and Eric D'Asaro. Ren-Chieh Lien and Eric Kunze both provided very helpful reviews of the manuscript. This work was funded by the National Science Foundation Grants 9819531 and 9819522.

REFERENCES

Alford, M. H., and R. Pinkel, 2000: Observations of overturning in the thermocline: The context of ocean mixing. *J. Phys. Oceanogr.,* **30,** 805–832.

Aucan, J., M. A. Merrifield, D. S. Luther, and P. Flament, 2006: Tidal mixing events on the deep flanks of Kaena Ridge, Hawaii. *J. Phys. Oceanogr.,* **36,** 1202–1219.

Batchelor, G. K., 1959: Small-scale variation of convected quantitites like temperature in turbulent fluid. *J. Fluid Mech.,* **5,** 113–139.

D'Asaro, E. A., and R.-C. Lien, 2000: The wave–turbulence transition for stratified flows. *J. Phys. Oceanogr.,* **30,** 1669–1678.

Dillon, T. M., 1982: Vertical overturns: A comparison of Thorpe and Ozmidov length scales. *J. Geophys. Res.,* **87,** 9601–9613.

Dugan, J. P., W. D. Morris, and B. S. Okawa, 1986: Horizontal wave number distribution of potential energy in the ocean. *J. Geophys. Res.,* **91,** 12 993–13 000.

Fleury, M., and R. Lueck, 1992: Microstructure in and around a double-diffusive interface. *J. Phys. Oceanogr.,* **22,** 701–718.

Galbraith, P. S., and D. E. Kelley, 1996: Identifying overturns in CTD profiles. *J. Atmos. Oceanic Technol.,* **13,** 688–702.

Gargett, A. E., 1985: Evolution of scalar spectra with the decay of turbulence in a stratified fluid. *J. Fluid Mech.,* **159,** 379–407.

Garrett, C. J. R., and W. H. Munk, 1975: Space-time scales of internal waves: A progress report. *J. Geophys. Res.,* **80,** 291–297.

Gregg, M. C., 1989: Scaling turbulent dissipation in the thermocline. *J. Geophys. Res.,* **94,** 9686–9698.

——, 1999: Uncertainties in measuring ε and χ_t. *J. Atmos. Oceanic Technol.,* **16,** 1483–1490.

——, and T. Meagher, 1980: The dynamic response of glass rod thermistors. *J. Geophys. Res.,* **85,** 2779–2786.

——, and T. Sanford, 1980: Signatures of mixing from Bermuda Slope, the Sargasso Sea, and the Gulf Stream. *J. Phys. Oceanogr.,* **10,** 105–127.

——, ——, and D. P. Winkel, 2003: Reduced mixing from the breaking of internal waves in equatorial waters. *Nature,* **422,** 513–515.

Henyey, F. S., J. Wright, and S. M. Flatté, 1986: Energy and action flow through the internal wave field. *J. Geophys. Res.,* **91,** 8487–8495.

Holbrook, W. S., and I. Fer, 2005: Ocean internal wave spectra inferred from seismic reflection transects. *Geophys. Res. Lett.,* **32,** L15604, doi:10.1029/2005GL023733.

Itsweire, E. C., T. Osborn, and T. Stanton, 1989: Horizontal distribution and characteristics of shear layers in the seasonal thermocline. *J. Phys. Oceanogr.,* **19,** 301–320.

Johnson, H. L., and C. Garrett, 2004: Efffects of noise on Thorpe scales and run lengths. *J. Phys. Oceanogr.,* **34,** 2359–2373.

Katz, E. J., 1975: Tow spectra from Mode. *J. Geophys. Res.,* **80,** 1163–1167.

——, and M. G. Briscoe, 1979: Vertical coherence of the internal wave field from towed sensors. *J. Phys. Oceanogr.,* **9,** 518–530.

Klymak, J. M., and M. C. Gregg, 2004: Tidally generated turbulence over the Knight Inlet sill. *J. Phys. Oceanogr.,* **34,** 1135–1151.

——, and J. N. Moum, 2007: Oceanic isopycnal slope spectra. Part I: Internal waves. *J. Phys. Oceanogr.,* **37,** 1215–1231.

——, and Coauthors, 2006: An estimate of tidal energy lost to turbulence at the Hawaiian Ridge. *J. Phys. Oceanogr.,* **36,** 1148–1164.

Kunze, E. L., L. K. Rosenfeld, G. S. Carter, and M. C. Gregg, 2002: Internal waves in Monterey Submarine Canyon. *J. Phys. Oceanogr.,* **32,** 1890–1913.

Lee, C. M., E. Kunze, T. B. Sanford, J. D. Nash, M. A. Merrifield, and P. E. Holloway, 2006: Internal tides and turbulence along the 3000-m isobath of the Hawaiian Ridge. *J. Phys. Oceanogr.,* **36,** 1165–1183.

Levine, E. R., and R. G. Lueck, 1999: Turbulence measurements with an autonomous underwater vehicle. *J. Atmos. Oceanic Technol.,* **16,** 1533–1544.

Levine, M. D., and T. J. Boyd, 2006: Tidally forced internal waves and overturns observed on a slope: Results from HOME. *J. Phys. Oceanogr.,* **36,** 1184–1201.

Lindborg, E., 2006: The energy cascade in a strongly stratified fluid. *J. Fluid Mech.,* **550,** 207–242.

MacKinnon, J., and M. Gregg, 2003: Shear and baroclinic energy flux on the summer New England shelf. *J. Phys. Oceanogr.,* **33,** 1462–1475.

Marmorino, G., 1987: Observations of small-scale mixing processes in the seasonal thermocline. Part II: Wave breaking. *J. Phys. Oceanogr.,* **17,** 1348–1355.

McKean, R. S., 1974: Internal wave measurements in the presence of fine-structure. *J. Phys. Oceanogr.,* **4,** 200–213.

——, and T. E. Ewart, 1974: Temperature spectra in the deep ocean off Hawaii. *J. Phys. Oceanogr.,* **4,** 191–199.

Moum, J. N., 1990: The quest for κ_ρ–preliminary results from direct measurements of turbulent fluxes in the ocean. *J. Phys. Oceanogr.,* **20,** 1980–1984.

——, 1996a: Efficiency of mixing in the main thermocline. *J. Geophys. Res.,* **101,** 12 059–12 069.

——, 1996b: Energy-containing scales of turbulence in the ocean thermocline. *J. Geophys. Res.,* **101,** 14 095–14 109.

——, and R. G. Lueck, 1985: Causes and implications of noise in oceanic dissipation measurements. *Deep-Sea Res.,* **32,** 379–390.

——, M. C. Gregg, R. C. Lien, and M. Carr, 1995: Comparison of turbulence kinetic energy dissipation rate estimates from two ocean microstructure profilers. *J. Atmos. Oceanic Technol.,* **12,** 346–366.

——, D. R. Caldwell, J. D. Nash, and G. D. Gunderson, 2002: Observations of boundary mixing over the continental slope. *J. Phys. Oceanogr.,* **32,** 2113–2130.

——, D. M. Farmer, W. D. Smyth, L. Armi, and S. Vagle, 2003: Structure and generation of turbulence at interfaces strained

by internal solitary waves propagating shoreward over the continental shelf. *J. Phys. Oceanogr.,* **33,** 2093–2112.

Nash, J. D., D. R. Caldwell, M. J. Zelman, and J. N. Moum, 1999: A thermocouple for high-speed temperature measurements in the ocean. *J. Atmos. Oceanic Technol.,* **16,** 1474–1483.

Osborn, T. R., 1980: Estimates of the local rate of vertical diffusion from dissipation measurements. *J. Phys. Oceanogr.,* **10,** 83–89.

——, and C. S. Cox, 1972: Oceanic fine structure. *Geophys. Fluid Dyn.,* **3,** 321–345.

——, and W. R. Crawford, 1980: An airfoil probe for measuring velocity fluctuations in water. *Air–Sea Interactions: Instruments and Methods,* F. Dobson, L. Hasse, and R. Davis, Eds., Plenum, 369–386.

——, and R. G. Lueck, 1985: Turbulence measurements from a towed body. *J. Atmos. Oceanic Technol.,* **2,** 517–527.

Polzin, K. L., J. M. Toole, and R. W. Schmitt, 1995: Finescale parameterizations of turbulent dissipation. *J. Phys. Oceanogr.,* **25,** 306–328.

Riley, J. J., and S. M. deBruynKops, 2003: Dynamics of turbulence strongly influenced by buoyancy. *Phys. Fluids,* **15,** 2047–2059.

Rosenblum, L. J., and G. Marmorino, 1990: Statistic of mixing patches observed in the Sargasso Sea. *J. Geophys. Res.,* **95,** 5349–5357.

Seim, H. E., and M. C. Gregg, 1997: The importance of aspiration and channel curvature in producing strong vertical mixing over a sill. *J. Geophys. Res.,* **102,** 3451–3472.

Smyth, W. D., J. N. Moum, and D. R. Caldwell, 2001: The efficiency of mixing in turbulent patches: Inferences from direct simulations and microstructure observations. *J. Phys. Oceanogr.,* **31,** 1969–1992.

Sreenivasan, K. R., 1996: The passive scalar spectrum and the Obukhov-Corrsin constant. *Phys. Fluids,* **8,** 189–196.

Tennekes, H., and J. L. Lumley, 1972: *A First Course in Turbulence.* The MIT Press, 300 pp.

Thorpe, S. A., 1977: Turbulence and mixing in a Scottish loch. *Philos. Trans. Roy. Soc. London,* **286A,** 125–181.